New Developments with C-Mn-Ni High-Strength Steel Weld Metals, Part A — Microstructure

A combination of high-resolution characterization techniques were employed to resolve complex microstructures

BY E. KEEHAN, L. KARLSSON, H.-O. ANDRÉN, AND H. K. D. H. BHADESHIA

ABSTRACT. The relationship between alloying content, microstructure, and properties has been clarified for high-strength steel weld metals with 7 to 9 wt-% nickel. Neural network modeling suggested that manganese reductions and nickel additions in a controlled manner with respect to manganese lead to increased impact toughness. Carbon additions were predicted to enhance yield strength at limited loss to impact toughness. Following these predictions, shielded metal arc welding was used to produce experimental welds with manganese at 0.5 or 2 wt-% and nickel at 7 or 9 wt-%, while carbon was varied between 0.03 and 0.11 wt-%. Based on Thermo-Calc calculations and the observed large nickel and manganese segregation to dendrite boundary regions, it was concluded that the weld metals solidified completely as austenite. High-resolution microscopy was used to characterize the microstructure. In high-manganese weld metals, a mixture of predominantly upper bainite and a coarse-grained constituent, characterized to be coalesced bainite was found in dendrite core regions. Mainly martensite was present at interdendritic regions. Manganese reductions were found to promote upper bainite while carbon additions were found to promote martensite. A constitutional diagram was constructed that summarizes microstructure as a function of manganese and nickel contents. In Part B of this work, the mechanical properties are presented and discussed in relation to the microstructure and the neural network predictions.

E. KEEHAN and L. KARLSSON are with ESAB AB, Gothenburg, Sweden. H.-O. ANDRÉN is with Department of Applied Physics, Chalmers University of Technology, Gothenburg, Sweden. H. K. D. H. BHADESHIA is with Department of Materials Science and Metallurgy, University of Cambridge, Cambridge, U.K.

Background

Steels with yield strengths in the region of 1000 MPa that possess good impact toughness have been readily available for some time. They are increasingly employed in many applications offering both size and weight reduction. In many circumstances, it is an engineering requirement that a weld metal with matching or overmatching strength is used. It is well known that maintaining good toughness becomes more problematic as strength levels increase above the region of 690 MPa (100 ksi) (Refs. 1, 2). As a result, there is a need to develop new high-strength welding consumables that meet the market requirements.

Metallurgists have addressed the challenges of increasing strength and toughness in steel through grain refinement, precipitation hardening, solid solution hardening, thermomechanical treatment, and the promotion of low-temperature transformation products such as martensite and bainite. Many have carried out research by varying elemental compositions or welding parameters with the aim of optimizing weld metal properties (Refs. 3–7). High-strength steel weld metals usually have carbon less than 0.2 wt-%, nickel less than 4 wt-%, and manganese less than 4 wt-% (Refs. 1, 7–22). Results generated yield strengths ranging from below 500 to above 1000 MPa. However, with the common flux shielded welding processes, good impact toughness was mostly achieved only at lower yield strengths.

For example, the promising work by Lord (Ref. 15) used the composition of a commercial shielded metal arc welding (SMAW) consumable (ESAB OK 75.78 with 3 Ni, 2 Mn, 0.5 Cr, 0.6 Mo, 0.05 C) as the basis of development. He increased nickel concentrations to 4 wt-% and decreased manganese levels to 0.8 wt-%. It was found that impact toughness increased to 74 J at –60°C, and the yield strength was reduced to 809 MPa (Ref. 15). Kang followed the trend of increasing nickel and reducing manganese with metal cored wires. He recorded an impact toughness of 55 J at –60°C with nickel at 6.95 wt-% and manganese at 0.52 wt-%. Tensile strength of 684 MPa was predicted for this alloy from hardness results. With microstructural investigations, the presence of lath martensite and various forms of ferrite was reported (Ref. 23). From literature, it is generally found that as impact toughness increases, yield and tensile strengths decrease. To limit strength losses, carbon additions and reducing interpass temperature have been most effective. For example, carbon levels up to 0.08 wt-% combined with 2–4 nickel and 1.4–2.0 manganese were found good for strength with limited losses in impact toughness (Refs. 24, 25). In another study, it was found that yield and ultimate tensile

KEYWORDS

High-Strength Steel
Neural Network Modeling
Shielded Metal Arc Welding
Impact Toughness
Segregation Behavior
Manganese Nickel

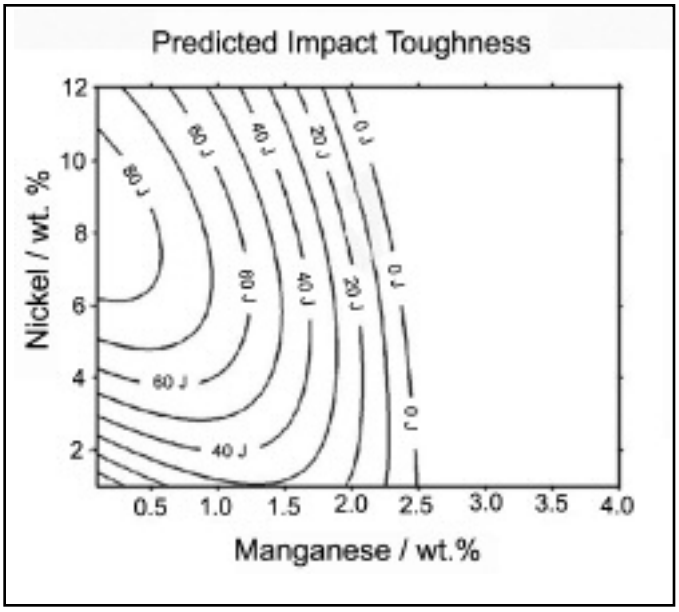

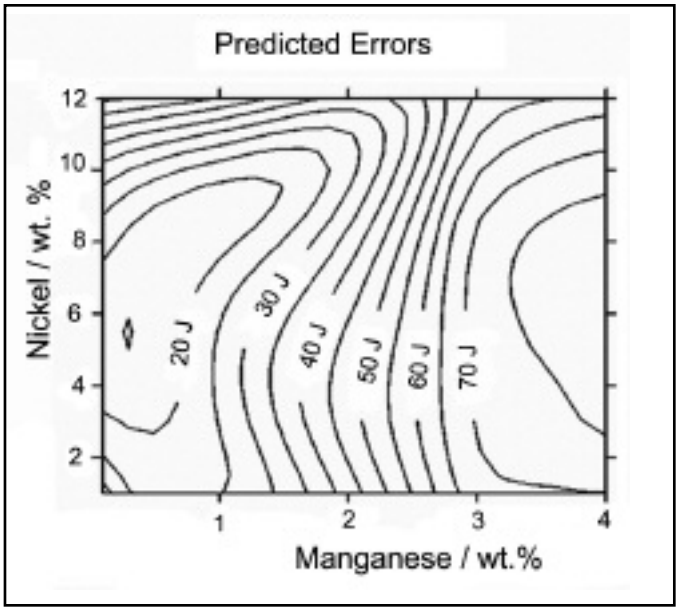

Fig. 1 — Contour plots showing the calculated weld metal impact toughness at –60°C as a function of manganese and nickel concentrations. The errors represent ± 1 σ of uncertainty. (Base composition as in Table 1.)

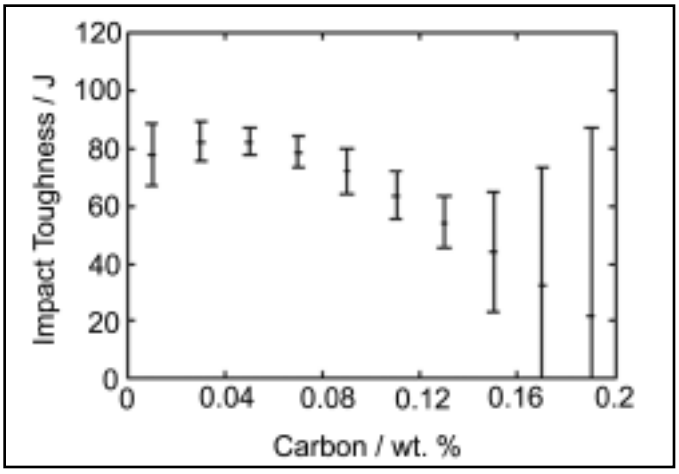

Fig. 2 — Predicted impact toughness at –60°C as a function of carbon concentration. The error bars represent ± 1 σ of uncertainty. (Base composition as in Table 1.)

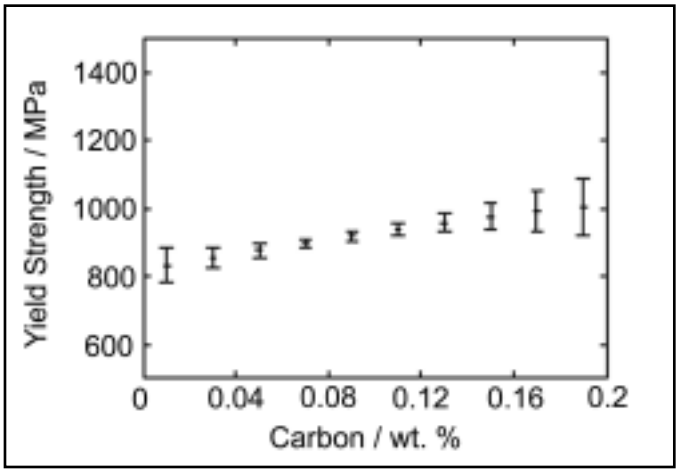

Fig. 3 — Predicted yield strength as a function of carbon concentration. The error bars represent ± 1 σ of uncertainty. (Base composition as in Table 1.)

strength also increased with decrease in interpass temperature (Ref. 25). In both cases, changes in mechanical properties were claimed to be strongly related to the microstructure described as mixtures of martensite and bainite.

With Lord's work (Ref. 15) as our starting point, neural network modeling was engaged to optimize the development process and to allow the effects of a wide variety of parameters to be perceived. The technique and the advantages it offers materials science are further described in Refs. 26–28. A brief description of the modeling applied in this research is given here and more complete details may be found in Refs. 29, 30. The present report is Part A of two reporting on work carried out on high-strength steel weld metals with variations in nickel, manganese, and carbon. Using SMAW, the effects were studied of varying nickel at 7 or 9 wt-%, manganese at 0.5 or 2.0 wt-%, and carbon between 0.03 and 0.11 wt-% on the microstructure (Part A) and the mechanical properties [Part B (Ref. 31)].

Neural Network Modeling

Neural network modeling is a powerful modeling method in which both input/output relationships (linear and nonlinear) can be captured directly from the data being modeled. In this project four neural network models were constructed to predict impact toughness, yield strength (YS), ultimate tensile strength (UTS), and elongation based on a database of some 3300 experimental weld metal results. Full details about the modeling may be found elsewhere (Ref. 30), and a brief summary is presented here.

Using the base composition presented in Table 1 along with an energy input of 1 kJ/mm and an interpass temperature of 250°C, a contour plot (Fig. 1) was generated for impact toughness behavior at –60°C for varied manganese and nickel. The predictions are surprising in that manganese reductions at all nickel levels lead to impact toughness increases. The contour plots also suggest that below a certain critical concentration of manganese, controlled additions of nickel can

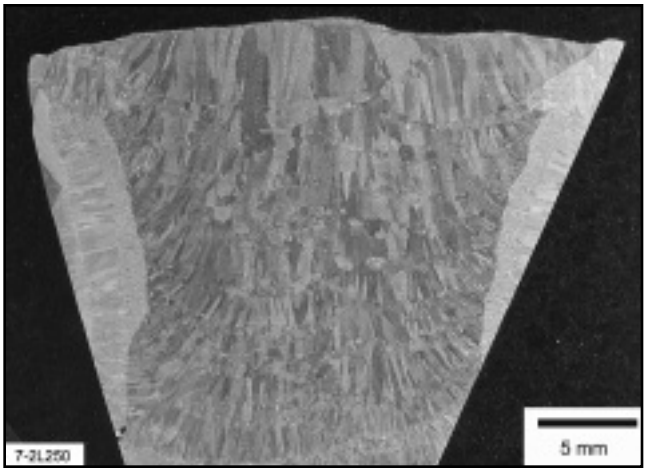

Fig. 4 — A low-magnification light optical micrograph from 7-2L250 showing a cross section of the welded joint.

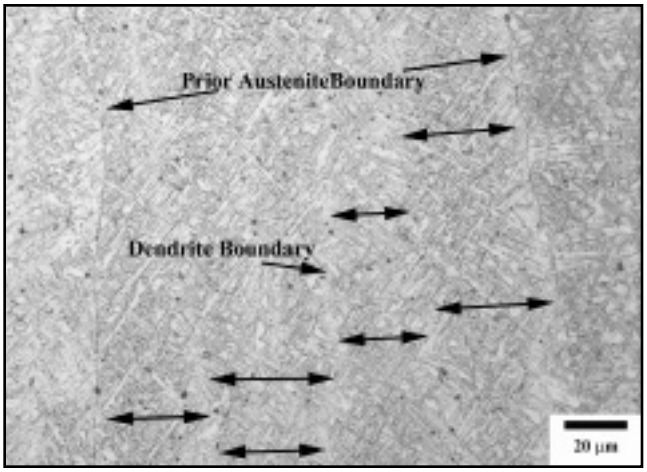

Fig. 5 — LOM micrograph from 7-0.5L200 showing a fine-scale microstructure. Here it is seen that dendrites formed within the columnar structure as the weld metal solidified.

Table 1 — The Base Composition Used for Analyzing the Effects of Nickel and Manganese Concentration in Neural Network Modeling[a]

Element	Content
C	0.034
Cr	0.50
Si	0.25
P	0.01
Mo	0.62
V	0.011
Cu	0.04
Co	0.009
W	0.005
S (ppm)	0.01
B (ppm)	1.00
Ti (ppm)	80
Nb (ppm)	10
O (ppm)	380
N (ppm)	250

(a) All elements are in wt-% unless otherwise stated.

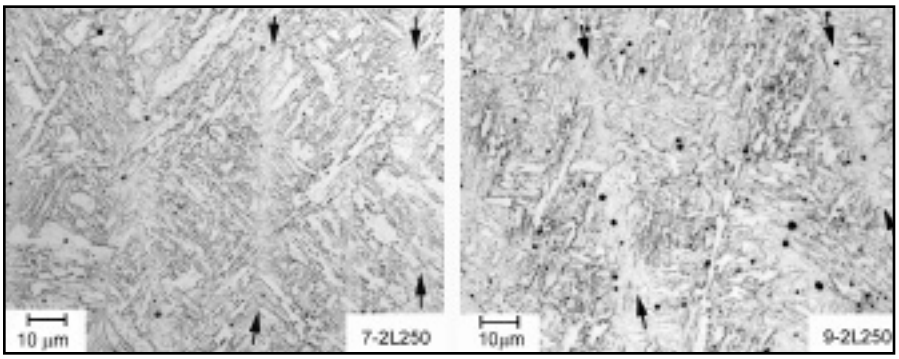

Fig. 6 — LOM micrographs of the as-deposited last bead from 7-2L250 and 9-2L250 showing a fine-scale microstructure with large grains not typically found in high-strength steel weld metals. The black arrows indicate the former dendrite boundaries.

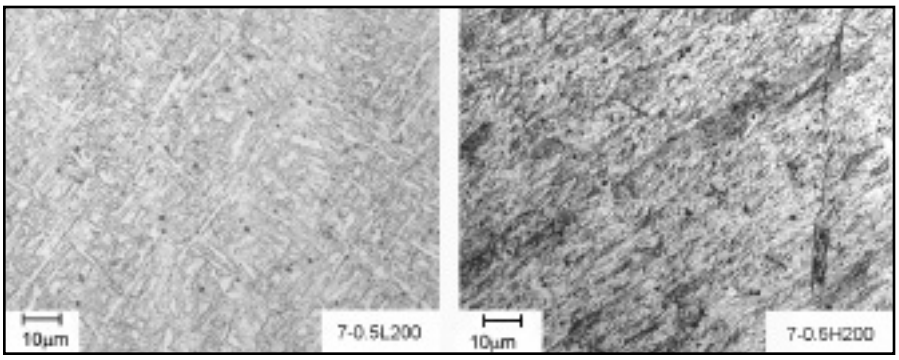

Fig. 7 — The refinement of the microstructure with increasing C content is clearly seen by comparing LOM micrographs of as-deposited last bead of 7-0.5L200 and 7-0.5H200.

lead to an increase in impact toughness as well as strength. However, the reverse mechanical behavior was predicted if nickel exceeds critical levels depending on the manganese concentration.

Given that the contour plot suggested the best impact toughness would be achieved with manganese and nickel concentrations in the region of 0.5 and 7.0 wt-%, respectively, the base input composition for further calculations was set at these values. Since it is well known that additions of carbon lead to strength increases, it was estimated with the models how yield strength and impact toughness would behave with carbon variations between 0 and 0.2 wt-%. The results of these predictions are presented in Figs. 2 and 3. It is shown that yield strength is predicted to increase from the region of 830 MPa to slightly over 1000 MPa when the carbon content is increased from 0.01 wt-% C to 0.19 wt-%. It was noted that impact toughness levels at –60°C are predicted to remain acceptable (47 J at –60°C) with carbon additions up to the region of 0.12 wt-%. Above this content, there are insufficient data to predict accurately (within ±10 J) as shown by large error bars.

Experimental Techniques

Based primarily on the neural network predictions, seven experimental weld met-

Table 2 — Welding Parameters and Chemical Composition (Welding parameters presented are energy input (E), interpass temperature (IPT), and the estimated cooling time beween 800° and 500°C ($t_{8/5}$) calculated from *WeldCalc* [Ref. 32])

Weld Metal	7-2L250	9-2L250	7-0.5L250	7-0.5L200	9-0.5L200	7-0.5M200	7-0.5H200
E/kJ mm–1	1.2	1.2	1.0	1.3	0.7	200	200
IPT/°C	250	250	250	200	200	200	200
t 8/5 /s	12	11	10	10	5	11	10
C(*)	0.032	0.031	0.024	0.00	0.026	0.061	0.110
Mn	2.02	2.11	0.64	0.61	0.37	0.56	0.53
Ni	7.23	9.23	6.60	6.11	8.67	6.84	7.04
Cr	0.47	0.48	0.21	0.16	0.20	0.15	0.14
Si	0.25	0.27	0.35	0.40	0.34	0.34	0.38
S(*)	0.008	0.008	0..008	0.009	0.008	0.006	0.007
P	0.011	0.011	0.012	0..01	0.007	0.011	0.008
Mo	0.63	0.64	0.40	0.38	0.41	0.35	0.40
V	n.a.	n.a.	n.a.	0.018	n.a.	0.014	0.016
Cu	0.03	0.03	0.03	0.02	0.01	0.01	n.a.
O (ppm)*	380	340	400	340	367	350	260
N (ppm)*	250	260	197	150	130	160	100

Composition is in wt-% unless otherwise stated.
* indicate elements analyzed using Leco combustion equipment.
n.a. = elements not analyzed.

als were produced using SMAW. It was decided to study the changes in mechanical and microstructural behavior in detail for manganese concentrations of 0.5 or 2.0 wt-%, nickel levels at 7 or 9 wt-%, and carbon additions from 0.03 to 0.11 wt-% with nickel at 7 wt-% and manganese at 0.5 wt-%. These compositional variations were chosen since modeling predicted significant effects on mechanical properties.

Welded joints were made according to ISO 2560 using 20-mm plates with a backing strip. The joints were buttered prior to the deposition of the experimental weld metals that took place in 33-cm runs with two or three runs per layer. An example of a typical cross section is shown in Fig. 4. The energy input and interpass temperature are presented in Table 2. Names were assigned to the weld metals according to composition and interpass temperature. Seven or 9 is the nickel content; 2 or 0.5 is the manganese content; L, M, or H are the low, medium, or high carbon contents; and 200 or 250 is the maximum interpass temperature. The estimated cooling time between 800° and 500°C ($t_{8/5}$) was calculated using the *WeldCalc* program (Ref. 32). Samples of weld metal were analyzed using a Spectro Lab S optical emission spectrometer and Leco combustion equipment (Model EF500 for C and S and Model TC–436 DR for N and O). The compositions of the weld metals are presented in Table 2.

Specimens from the weld metal cross section, extracted perpendicular to the welding direction, were mounted in bakelite, wet ground, polished to 1-μm diamond paste and etched using 2% nital etchant for analysis with light optical microscopy (LOM) and field emission gun scanning electron microscopy (FEGSEM). A Leitz Aristomet light optical microscope and a Leo Ultra 55 FEGSEM were used in these examinations. Polished specimens were examined with scanning electron microscopy (SEM) in the backscattered mode and elemental analysis was carried out using energy-dispersive X-ray analysis (EDX). For TEM studies, 3-mm disc shape samples, perpendicular to the welding direction, were ground to between 50 and 80 μm in thickness and then jet electropolished at –35°C using 10% perchloric acid in methanol. After electropolishing, the specimens were further thinned by ion beam milling for a few minutes at a low angle using a Gatan precision ion polishing system (PIPS). These specimens were examined with a Jeol 2000 FX or a Philips CM200 TEM.

Dilatometer specimens in the form of cylinders with a diameter of 3 mm and a length of 10 mm were machined from the center of the welded joint. These were then investigated using a Theta Dilatronic III dilatometer. The specimens were heated to 1000°C at a rate of 25°C/s, held for 5 minutes and afterward cooled to room temperature at different cooling rates. Individual samples were used for each cooling rate.

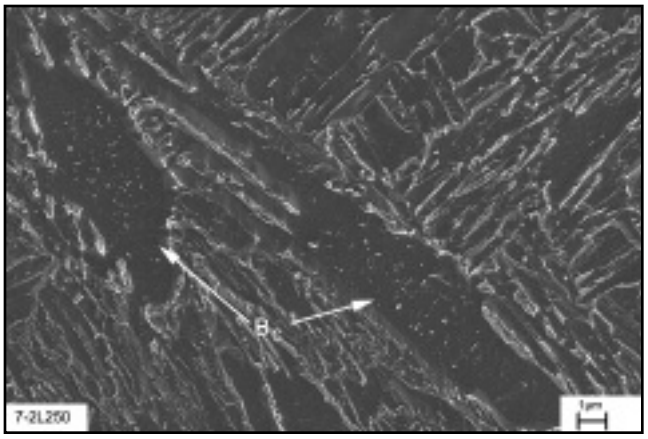

Fig. 8 — Coalesced bainite in weld metal 7-2L250. Small precipitates can be observed within the bainitic ferrite grains.

Results

Microstructure – The Last Bead

The welded joints comprised different regions and the microstructure of the joint was inhomogeneous from region to region — typical of a normal welded joint. The last bead of each weld was found to consist of a columnar structure with the columns varying in size but normally less than 0.5 mm in width — Fig. 4. These columns were further subdivided into a cellular structure of dendrites with a thickness between 10 and 30 μm — Fig. 5.

Light optical micrographs in Figs. 6 and 7 present the variation of microstructure in the as-deposited last bead as a result of changing nickel and carbon content. In the images the former dendrite

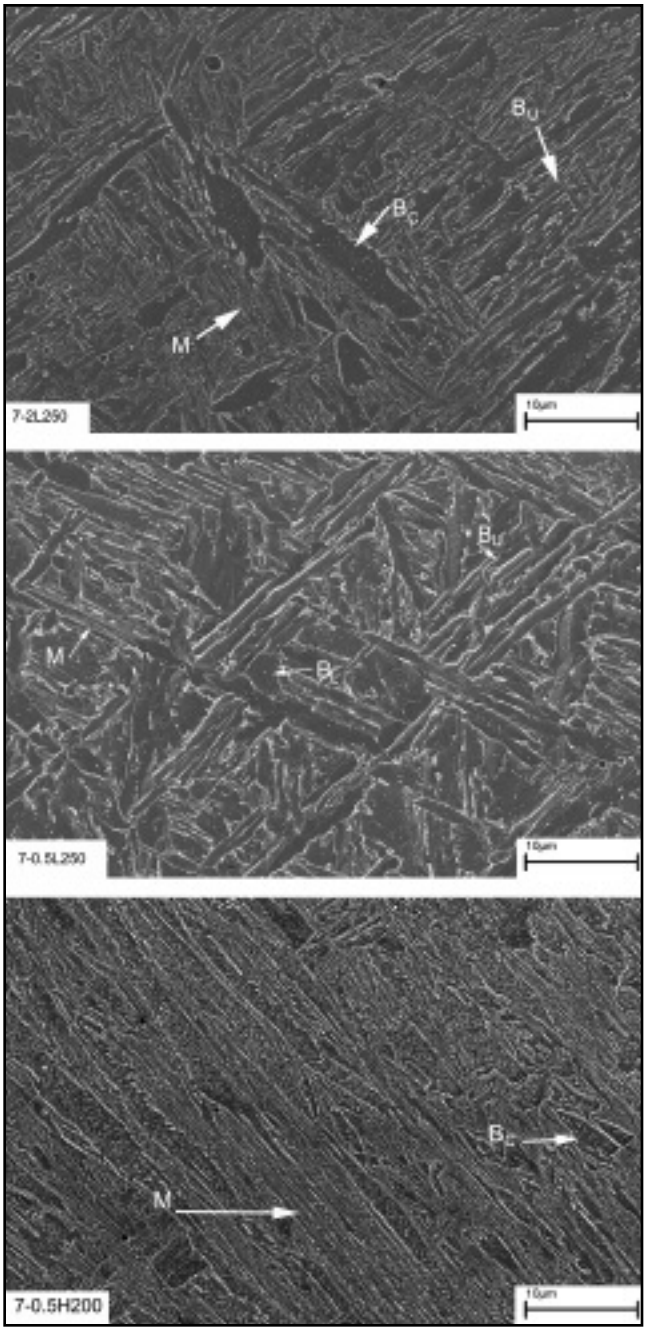

Fig. 9 — The microstructures in the as-deposited last bead of weld metals 7-2L250, 7-0.5L250, and 7-0.5H200 imaged using FEGSEM. M is for martensite, B_U is upper bainite, B_L is lower bainite, and B_C is coalesced bainite.

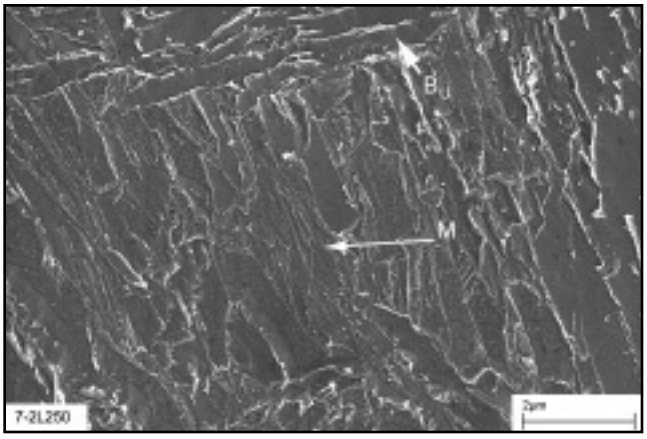

Fig. 10 — An interdendritic region in the last bead of weld metal 7-2L250 showing a mainly martensitic microstructure. M is martensite and B_U is upper bainite.

boundaries can be seen. The microstructure is very fine scale, typical of martensite or bainite, but it is not possible to decipher between the two with LOM due to their similar morphologies. Large grains not commonly found in high-strength steel weld metals were also observed in particular with 7-2L250 and 9-2L250. LOM images from the as-deposited last bead in 7-0.5L200 and 7-0.5H200 are shown in Fig. 7, which allows the effect of changing carbon from 0.03 to 0.11 wt-% to be observed. It was found that the microstructure becomes very fine with an increase of carbon content, but again, it is not possible with LOM to identify the microstructure with full certainty and investigations with instruments offering better resolution are necessary. This work has been carried out with FEGSEM and TEM and full details may be found elsewhere (Refs. 33–36). A summary is presented here.

The microstructure was resolved to be mainly a mixture of martensite and upper and lower bainite along with an uncommon coarse-grained variant of bainite — coalesced bainite. Figure 8 shows a FEGSEM image of coalesced bainite in weld metal 7-2L250. Coalesced bainite has previously been reported in several high-strength steels (Ref. 37) and is believed to form through coalescence of individually nucleated bainitic ferrite platelets with identical crystallographic orientation during prolonged growth (Ref. 38). Coalescence have been observed for relatively low transformation temperatures when the driving force is large as when M_s and B_s are close to each other (Ref. 38). It can develop to have a large grain size and is considered negative for mechanical properties. Full details about coalesced bainite and its characterization are presented elsewhere (Ref. 36).

In Fig. 9, the as-deposited last bead microstructures of weld metals 7-2L250, 7-0.5L250, and 7-0.5H200 are shown. The effects of reducing manganese content from 2 to 0.5 wt-% at nickel content of 7 wt-% may be observed by comparing the micrographs from 7-2L250 and 7-0.5L250. With 7-0.5L250 there was the noticeable absence of coalesced bainite, and the microstructure was predominately upper and lower bainite in former dendrite core regions, while martensite was the main constituent at interdendritic regions. Comparing 7-0.5L250 and 7-0.5H200, it was found that carbon additions promote a finer microstructure with mainly martensite across the dendrites (Fig. 9) (Ref. 35).

A more detailed study of weld metal 7-2L250 illustrates the local variation of microstructure within a bead. In this weld metal generally coalesced bainite was found along with upper bainite in dendrite core regions (Figs. 8 and 9), while a lath-like microstructure of martensite was found at interdendritic regions. An interdendritic region is shown at higher magnification in Fig. 10 where the morphology of martensite can be seen. It is also observed that a small distance away from the interdendritic region upper bainite forms. Overall, it was found that the microstructure in weld metal 9-2L250 was similar to that of 7-2L250 with the same microstructural constituents developing, but with less coalesced bainite and more martensite (Ref. 33).

Given the high nickel content, it was decided to measure retained austenite content using X-ray diffraction. Only minor amounts were confirmed, with less than 2 vol-% reported in all weld metals (Ref. 30).

Table 3 — Average Compositions Recorded in wt-% at Dendritic Boundary Regions and Dendrite Core Regions in the Last Bead Using EDX Spot Analysis (Mn value in brackets are values adjusted using the average composition in Table 2 to allow for the overestimation of Mn with EDX).

Weld Metal	Mn	Ni
7-2L250 Boundary	3.1 (2.5)	8.18
7-2L250 Core	2.35 (1.75)	6.30
9-2L250 Boundary	3.2 (2.9)	10.30
9-2L250 Core	2.05 (1.75)	7.70
7-0.5L250 Boundary	0.95 (0.9)	7.55
7-0.5L250 Core	0.57 (0.5)	5.83

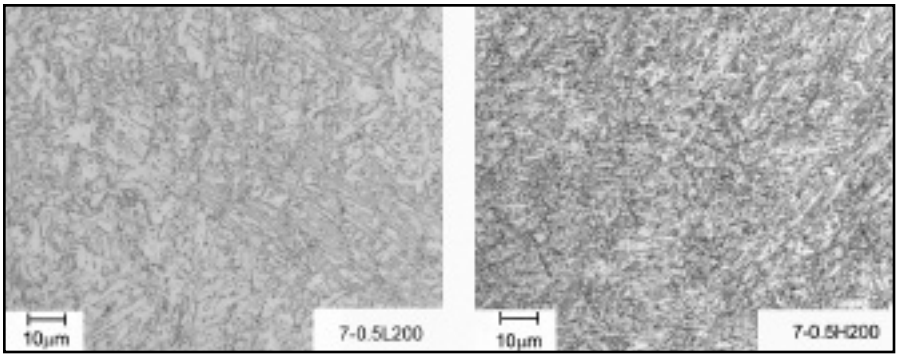

Fig. 11 — LOM micrographs from 7-0.5L200 and 7-0.5H200 showing the microstructure in the bead interior of reheated central beads in the joint.

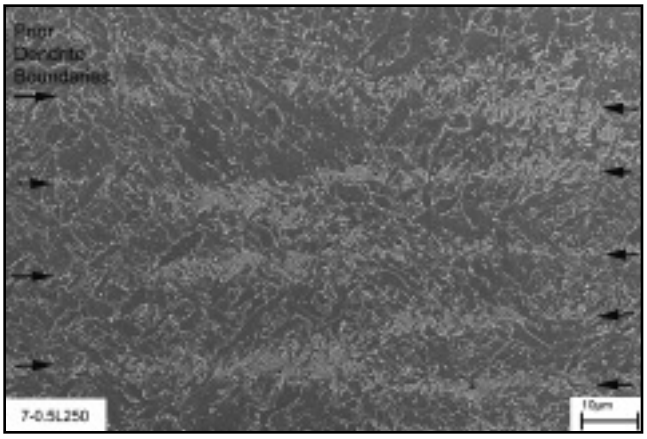

Fig. 12 — A FEGSEM overview of a reheated bead in weld metal 7-0.5L250.

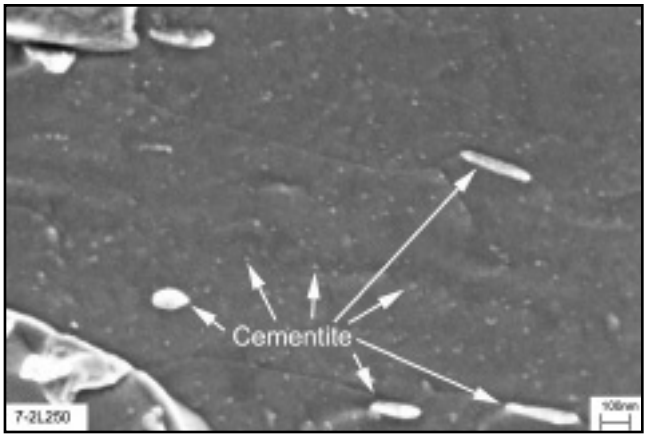

Fig. 13 — A high-magnification FEGSEM micrograph showing spheroidized and coarsened cementite along with newly formed small precipitates in tempered bainite in a reheated bead of weld metal 7-2L250.

Microstructure — Reheated Beads

The microstructure in central beads was, as expected, even more complex as a result of their complicated and varying thermal histories depending on the location within the joints. In particular with LOM and also with FEGSEM images, it is often difficult to identify the microstructural constituents. An example is shown in Fig. 11 that presents the center of reheated beads in weld metals 7-0.5L200 and 7-0.5H200. However, in combination with examinations and knowledge of the microstructure in the last bead (Fig. 9), the microstructure can be inferred to be that of mainly tempered bainite with 7-0.5L200 and mainly tempered martensite with 7-0.5H200.

The importance of understanding the last bead is also illustrated in Fig. 12, which shows an overview of the center in a reheated bead in weld metal 7-0.5L250. Within the micrograph, the former dendrites are clearly seen. The same microstructural variation was found across the former dendrites, as in the last bead, except that it was tempered. In dendrite core regions, mainly tempered bainite (Fig. 13) was found while tempered martensite (Fig. 14) was predominantly found at interdendritic regions. In bainitic areas it was found that the carbon had redistributed within the bainitic ferrite. The cementite precipitates observed in the last bead (Fig. 8) were found to have spheroidized within the grains and coarsened at the grain boundaries. In addition very small cementite precipitates in the order of a few nanometers had formed within the bainitic ferrite. These latter precipitates along with the former spheroidized and coarsened precipitates were confirmed to be cementite using TEM and electron diffraction (Refs. 33, 39).

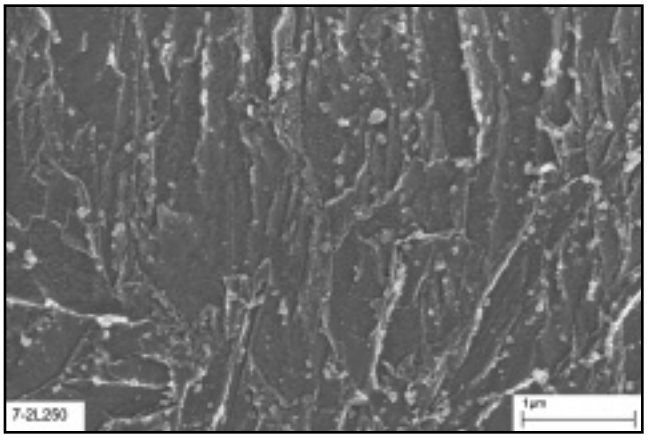

Fig. 14 — FEGSEM image of tempered martensite in a former interdendritic region within a reheated bead of weld metal 7-2L250.

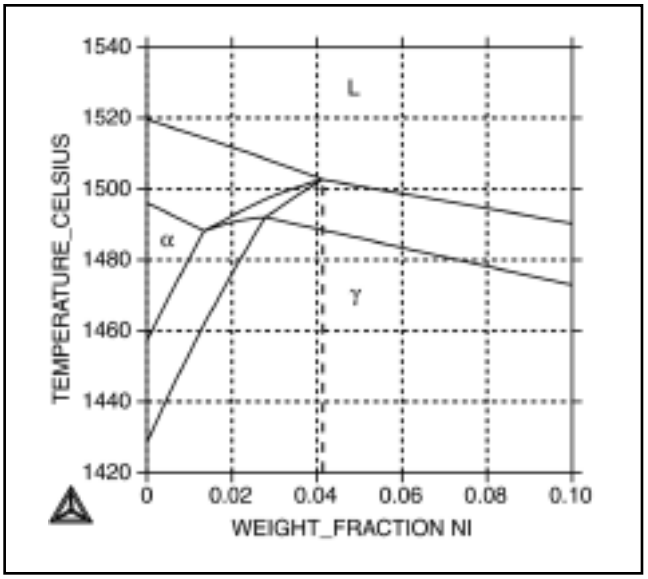

Fig. 15 — Isopleth as a function of nickel content and temperature based on the composition of weld metal 7-2L250 calculated using Thermo-Calc.

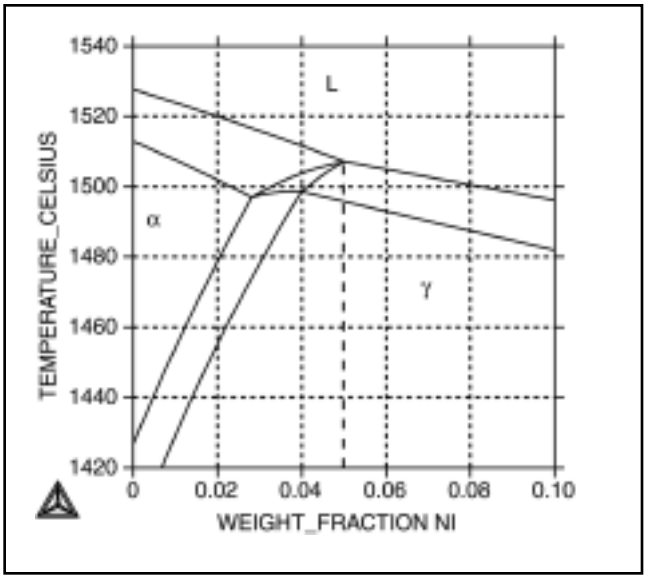

Fig. 16 — Isopleth calculated with Thermo-Calc *for the composition of weld metal 7-0.5L250 as a function of nickel content and temperature.*

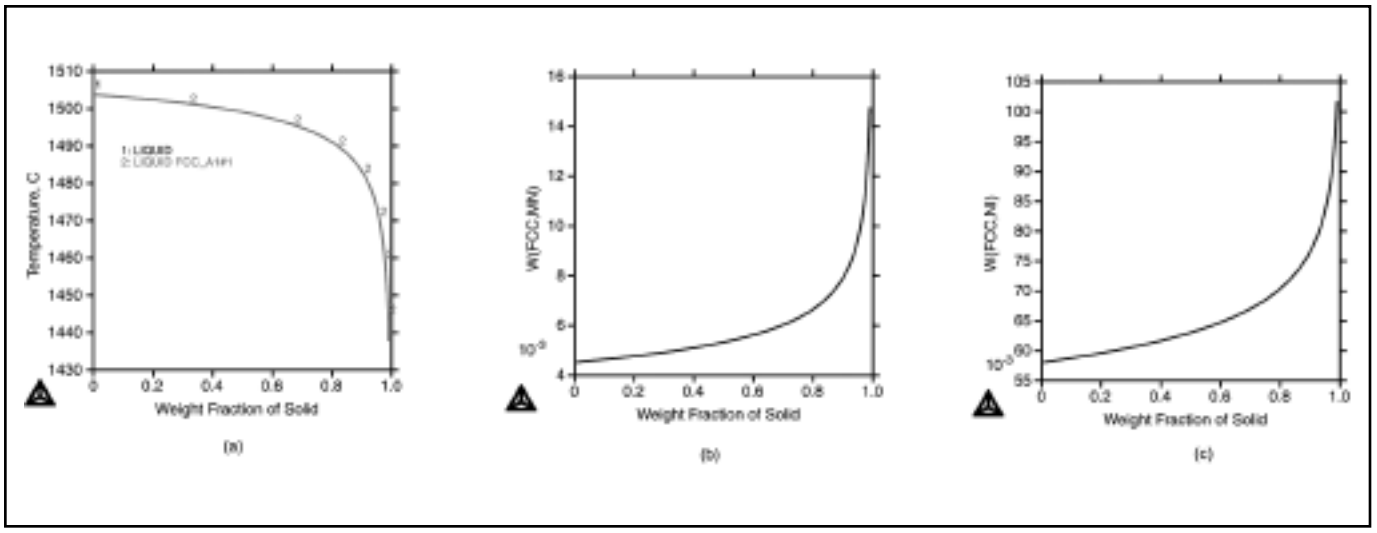

Fig. 17 — Scheil simulations for weld metal 7-0.5L250 of the following: A — The weight fraction of solid and liquid as a function of temperature; B — manganese content as a function of the weight fraction of solid; and C — nickel content as a function of the weight fraction of solid.

Dilatometry

Transformation temperatures for the different weld metals are presented in Table 4. The results at cooling rates of 25–40°C/s are representative of the cooling rates within the welded joints based on $t_{8/5}$ calculations. Generally, it can be said that greater alloying content with nickel, manganese, and carbon stabilize austenite to lower temperatures. Overall there was no large difference in austenite transformation temperature as a result of changing the cooling rate.

It is seen by comparing 7-2L250 and 9-2L250 that nickel additions reduce both Ac_1 and Ac_3 temperatures and on cooling austenite is stabilized to lower temperatures. Comparing 7-2L250 and 7-0.5L250, it is found that a reduction in manganese content increases both Ac_1 and Ac_3 temperatures and austenite transformation on cooling takes place in the region of 100° higher. Carbon additions were found to reduce the Ac_1 temperature, but interestingly, Ac_3 was maintained at the same temperature as with low carbon levels (cf. 7-05L250 and 7-05H200 in Table 4). Austenite was stabilized to very low temperatures on cooling (365°C), the same transformation temperature as with high nickel and manganese.

Elemental Segregation

When polished specimens from weld metals 7-2L250, 9-2L250, and 7-0.5L250 were examined in the backscattered mode, there was a clear contrast between the dendrite core regions and the interdendritic, regions. This led to the observation that there may be significant elemental segregation across the former dendrites and it was decided to carry out EDX analysis. The results are presented in Table 3. In

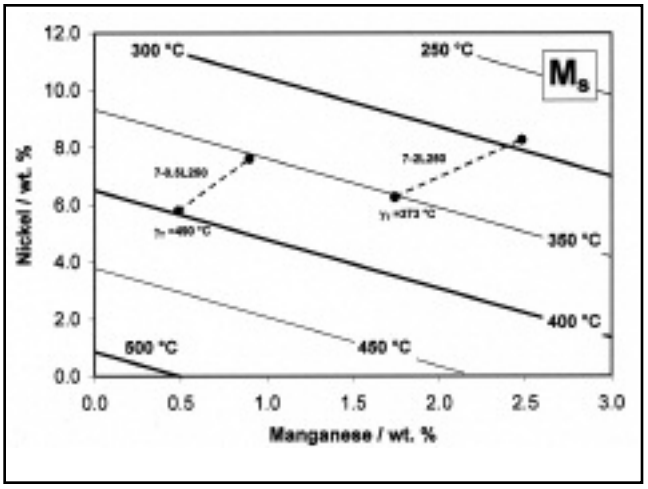

Fig. 18 — The martensite start temperature (M_s) as a function of manganese and nickel content calculated for the base composition in Table 1 using the M_s empirical equation (Ref. 42). Also plotted is the variation in alloying content between interdendritic (richer contents) and dendrite core regions (leaner contents) for 7-2L250 and 7-0.5L250. The austenite transformation temperatures (γ_T) recorded with dilatometry are also shown.

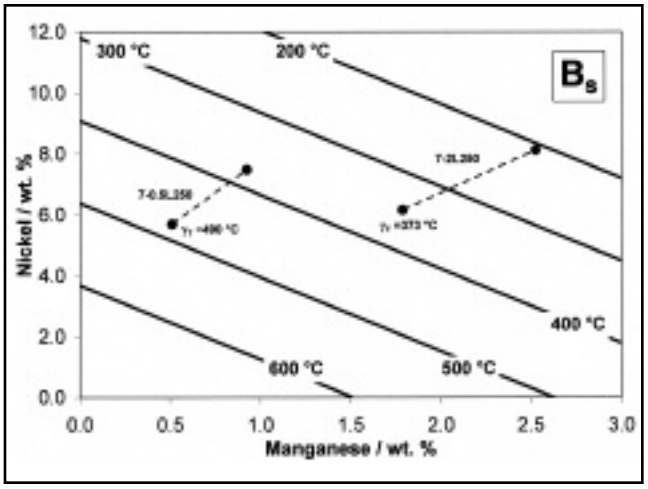

Fig. 19 — The bainite start temperature (B_s) as a function of manganese and nickel content calculated for the base composition in Table 1 using the B_s empirical equation (Ref. 41). The austenite transformation temperatures (γ_T) recorded with dilatometry specimens are shown for weld metals 7-2L250 and 7-0.5L250, along with the variation in alloying content between interdendritic (richer contents) and dendrite core regions (leaner content).

general, it was found that manganese was overestimated in all analyses. Nevertheless, it was observed that interdendritic regions were enriched in nickel and manganese with weld metal 9-2L250 showing the greatest amounts of segregation.

Thermo-Calc Calculations

Given that it is difficult to observe with microstructural studies whether the weld metals solidified as ferrite or austenite, it was decided to use *Thermo-Calc* (Ref. 40) to simulate the transformation based on alloying content. It was felt that the solidification mode is of particular importance for the amount of segregation that will take place and knowledge of it was necessary to have a complete understanding of the final microstructure.

Predictions from *Thermo-Calc* were made using the CCTSS database and are presented in Figs. 15–17. The liquid to solid transformation as a function of nickel content and temperature for the base compositions of weld metals 7-2L250 and 7-0.5L250 are presented as isopleths in Figs. 15 and 16, respectively. Comparing the diagrams, it is seen that ferrite can form during solidification at higher nickel contents with the lower manganese content. However, even with 0.5 wt-% manganese, it was observed that at all nickel contents in the weld metals presented in Table 2 fully austenitic solidification will take place.

Figure 17 presents Scheil simulations for 7-0.5L250. In these calculations, it is assumed that no diffusion occurs in the solid state after solidification and that the liquid is fully in equilibrium. In diagram A, the weight fraction of solid is predicted as a function of temperature. In B, the weight fraction of manganese content as a function of the weight fraction of solid is predicted, while in C the weight fraction of nickel content as a function of the weight fraction of solid is shown.

Table 4 — Austenite Decomposition Temperatures Recorded Using Dilatometry

Weld Metal	Ac_1/°C	Ac_3/°C	Transformation of γ 25°–40°C/s cooling	Transformation of γ 1°C/s cooling
7-2L250	690	740	373	390
9-2L250	665	720	365	365
7-0.5L250	700	770	490	480
7-0.5H200	685	770	355	365

Discussion

Solidification and Segregation

From *Thermo-Calc* simulations it was suggested that all the experimental weld metals solidified completely as austenite. Solidification as austenite may explain why the former dendritic structure is so clearly visible within the microstructure. Once solidification has taken place, diffusion of substitutional elements is much more limited in the austenitic lattice than in the ferrite lattice. The local chemistry at high temperatures is therefore inherited down to lower temperatures and thus may affect low-temperature phase transformations.

An interesting comparison to make is between the Scheil simulations presented in Fig. 19 and the EDX spot analysis results presented in Table 3. From the Scheil calculations for the weld metal 7-0.5L250 composition, it is predicted that the first solid to form has 0.45 wt-% manganese and 5.8 wt-% nickel (dendrite core regions) while the final composition to solidify is estimated to be 1.5 wt-% manganese and 10.2 wt-% nickel (interdendritic regions). Comparing these figures with EDX results, the average manganese and nickel contents of the first solid to form was 0.57 and 5.83 wt-%, respectively, (dendrite core region) and the last solid to form had 0.95 wt-% man-

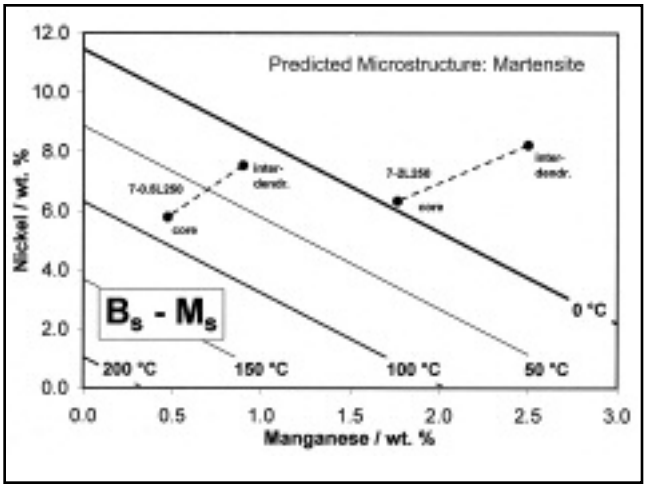

Fig. 20 — The difference between B_s and M_s as a function of manganese and nickel content calculated using the B_s and M_s empirical equations (Refs. 41, 42) along with the base composition in Table 1. The compositional variations between interdendritic and dendrite core regions are illustrated for 7-0.5L250 and 7-2L250.

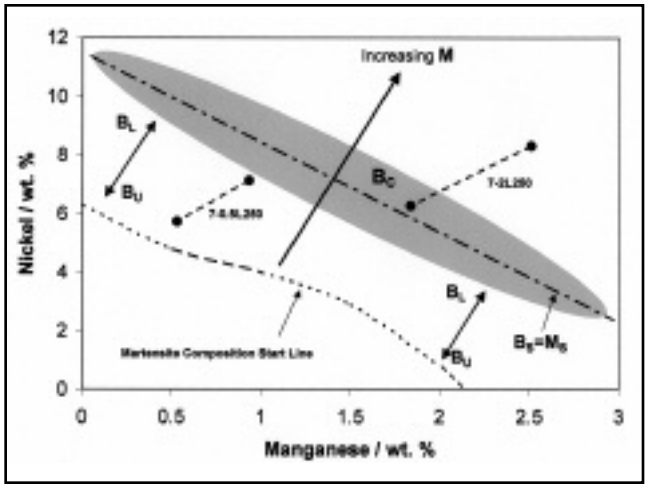

Fig. 21 — Constitutional diagram showing the dominant microstructure as a function of nickel and manganese content for the base composition 0.034 C, 0.25 Si, 0.5 Cr, and 0.62 Mo. The martensite composition start line is taken from literature (Ref. 44). Also shown is the line where B_s and M_s are calculated to be equal using empirical equations (Refs. 41, 42).

ganese and 7.55 wt-% nickel. From this comparison, it is seen that there is fairly good agreement between the simulations and the actual measured alloying content considering the spatial resolution of EDX analysis and the fact that some diffusion will take place. Similar agreement was found for Alloys 7-2L250 and 9-2L250, supporting the conclusion that the weld metals solidified as austenite.

Given that a greater alloying content is found at interdendritic regions, phase transformations and the final microstructure will be affected. With knowledge of the effects of alloying content, the variation in microstructure both across the dendrites and between the alloys can be understood and justified as will be discussed in the following section.

Microstructural Constituents

It was found that carbon additions from 0.03 to 0.11 wt-%, at 0.5 wt-% manganese and 7 wt-% nickel reduced austenite transformation temperature from 490 to 355°C. In doing so, the microstructure became mainly martensitic (Fig. 9) with some bainite also forming in dendrite core regions. Calculating the martensite start temperature (M_s) and the bainite start temperature (B_s) using the empirical equations $M_s = 539 – 423$ (%C) – 30.4 (%Mn) – 17.7 (%Ni) – 12.1 (%Cr) – 7.5 (%Mo) and $B_s = 830 – 270$ (%C) – 90 (%Mn) – 37 (%Ni) – 70 (%Cr) – 83 (%Mo) (Refs. 41, 42), it is seen that the predicted B_s of the low-carbon weld metal of 498°C agrees very well with the measured transformation temperature of 490°C. For the high-carbon variant, the calculated M_s is 347°C, which is also close to the measured transformation temperature of 355°C. Clearly, predicted and measured transformation temperatures (Table 4) are in good agreement taking into account the observed dominant microstructural constituents.

Given the good agreement, it was decided to visualize the effect of alloying content on the M_s and the B_s temperatures. Plots (Figs. 18 and 19) were made using the M_s and the B_s equations (Refs. 41, 42) as a function of manganese and nickel content along with the base input composition of Table 1. With greater alloying contents, both the martensite start temperature M_s and bainite start temperature B_s are suppressed to lower temperatures. The distances between the iso-M_s and iso-B_s lines are different. Also plotted in both figures is the variation in alloying content between interdendritic and dendrite core regions as measured using EDX (Table 3) for weld metals 7-2L250 and 7-0.5L250 along with the recorded transformation start temperature from dilatometry measurements (Table 4). When the difference between the two temperatures is plotted as shown in Fig. 20, it is found that M_s and B_s are approximately equal along a line passing through the alloying content of 2 wt-% manganese and 7 wt-% nickel. Reducing manganese or nickel is predicted to promote bainite while increasing manganese or nickel will promote the formation of martensite.

Interestingly, the coarse-grained constituent coalesced bainite was only observed for weld metal compositions having a low transformation temperature with B_s and M_s close to each other [dilatometry (Ref. 39)]. Coalesced bainite was most clearly seen in weld metal 7-2L250 having an austenite transformation temperature of 373°C (Table 4). The microstructure in this weld metal was a mixture of upper bainite along with coalesced bainite in dendrite core regions while martensite was found at interdendritic regions (Figs. 8–10). As illustrated in Fig. 20, the B_s and M_s temperatures are predicted to be close for the composition of the dendrite core regions (Table 3), where coalesced bainite was observed. A complete discussion about coalesced bainite may be found elsewhere (Refs. 36, 38, 39).

The differences in microstructure across the dendrites in weld metal 7-2L250 may be explained in terms of the local composition variation (Table 3). Interdendritic regions, which were enriched in alloying content, are believed to transform at lower temperatures predominantly to martensite. This is in agreement with dilatometry experiments and predictions of B_s and M_s — Figs. 18–20.

Reducing manganese content with weld metal 7-0.5L250 was found to promote austenite transformation at a higher temperature (in the region of 490°C, Table 4). In this weld metal the microstructure was that of mainly upper and lower bainite in dendrite core regions as shown in Fig. 9, with some little martensite forming at interdendritic regions.

Finally, based on microstructural observations, dilatometry experiments, M_s and B_s predictions, and literature data, a constitutional diagram was constructed showing the dominant microstructural constituents as a function of nickel and manganese content. In Fig. 21, mi-

crostructural regions are shown together with the martensite composition start line taken from literature (Ref. 43). Also plotted is the line where B_s and M_s are equal (where B_C is expected to form). In conclusion, all microstructural observations for the 7 or 9 nickel weld metals, including effects of segregation, are in excellent agreement with the proposed constitutional diagram. However, it should be kept in mind when applying the diagram that effects of variation in cooling rate and changes in alloying elements other than manganese and nickel also have to be considered.

Transformation Behavior on Tempering

Dilatometry experiments showed that changes in nickel, manganese, and carbon content give a variation in Ac_1 and Ac_3 temperatures. With greater nickel content, austenite formed earlier on reheating while reducing manganese was found to increase Ac_1 and Ac_3 to higher temperatures. Carbon additions with 7 wt-% nickel and 0.5 wt-% manganese were found to reduce Ac_1 slightly, but had no effect on Ac_3. Although the changes in Ac_1 and Ac_3 are not that large, nevertheless they will have an effect on the relative amount of tempered microstructure within the welded joints as well as the degree of tempering. Lower Ac_1 and Ac_3 temperatures give greater amounts of stronger freshly formed microstructural constituents while higher Ac_1 and Ac_3 promote more tempering, which is likely to give a tougher microstructure. Possible effects on strength and impact toughness are discussed in Part B (Ref. 31).

Conclusions

Neural network modeling explored compositions with a potential to offer increased strength while maintaining impact toughness in high-strength steel weld metals. Based on the predictions, experimental welds were made using SMAW with manganese at 0.5 or 2.0 wt-% and nickel at 7 or 9 wt-%. Additional welds were made where carbon was varied between 0.03 and 0.11 wt-% with manganese set at 0.5 wt-% and nickel at 7 wt-%.

From *Thermo-Calc* modeling and observed segregation behavior, it was concluded that the weld metals solidified completely as austenite.

Nickel and carbon additions were found to stabilize austenite to lower transformation temperature, while manganese reductions promote the decomposition of austenite at higher temperatures.

Combinations of high-resolution microstructural characterization techniques were employed to assess the microstructures. For a combination of high nickel and manganese, a mixture of upper and coalesced bainite was found in dendrite core regions with mainly martensite present in interdendritic regions. A manganese reduction reduced the amount of coalesced bainite and promoted greater amounts of upper bainite within the microstructure while carbon additions were found to promote martensite.

A constitutional diagram has been constructed summarizing the effects on microstructure of varying manganese and nickel contents.

Acknowledgments

Prof. L.-E. Svensson of Chalmers University of Technology is thanked for fruitful discussions. M. Murugananth, formally of University of Cambridge, is thanked for producing neural network predictions. K. Frisk and A. Markström of the Swedish Institute of Metals Research are thanked for producing *Thermo-Calc* predictions. ESAB AB is thanked for the production of experimental weld metals, permission to publish results, and financial support. Knowledge Foundation of Sweden is thanked for additional financial support. The FEGSEM instrument was financed by a grant from the Knut and Alice Wadenberg Foundation.

References

1. Svensson, L. E. 1999. Consumables for welding high-strength steels. *Svetsaren* 54(1–2): 29–33.

2. Widgery, D. J., Karlsson, L., Murugananth, M., and Keehan, E.2002. Approaches to the development of high-strength weld metals. *Proceedings 2nd Int. Symposium on High-Strength Steel*. Stiklestad, Verdal, Norway: European Coal and Steel Community (ECSC), B-1049 Brussels, Belgium.

3. Leslie, W. C. 1981. *The Physical Metallurgy of Steels*. London, U.K.: McGraw - Hill.

4. *ASM Handbook*, 10th ed., Vol. 1. 1990. Properties and selection of iron, steel and high performance alloys. Materials Park, Ohio: ASM International.

5. Davies, A. C. 1992. Welding science and technology. 10 ed. *The Science & Practice of Welding*. Vol. 1. Cambridge University Press.

6. Svensson, L.-E. 1994. *Control of Microstructure and Properties in Steel Arc Welds.* CRC Press, Inc.

7. Evans, G. M., and Bailey, N. 1997. *Metallurgy of Basic Weld Metal.* Abington Publishing.

8. Abson, D. J., and Pargeter, R. J. 1986. Factors influencing as-deposited strength, microstructure, and toughness of manual metal arc welds suitable for C-Mn steel fabrications. *International Metals Reviews* 31(4): 141–194.

9. DeLoach, J. 1990. *Microstructural Features Controlling Ductile-to-Brittle Transition Behavior in High-Strength, Martensitic Steel Weld Metals.* AD-A229 948/5/XAB: p. 122.

10. Fleming, D. A., Bracarense, A. Q., Liu, S., and Olson, D. L. 1996. Towards developing a SMA [MMA] welding electrode for HSLA [high-strength, low-alloy] 100 grade steel. *Welding Journal* 75(6): 171-s to 183-s.

11. Grong, O., and Matlock, D. K. 1986 Microstructural development in mild and low-alloy steel weld metals. *Int. Met. Rev.* 31(1): 27–48.

12. Harrison, P. L., and Farrar, R. A. 1987. Microstructural development and toughness of C-Mn and C-Mn-Ni [steel] weld metals. Part 1: Microstructural development. *Metal Construction* 19(7): 392R–399R.

13. Lau, T. W., Sadowsky, M. M., North, T. H., and Weatherly, G. C. 1987. Effect of nitrogen on the toughness of HSLA weld deposits in welding metallurgy of structural steels. *International TMS/EWI Symposium*, Denver, Colo. Warrendale, Pa.: Metallurgical Society of AIME (TMS).

14. Liao, J., Kametani, H., Okada, H., and Ikeuchi, K. 2001. Toughness of weld metals of 950 MPa high strength steel. *7th Int. Symposium, Today and Tomorrow in Science and Technology of Welding and Joining*. Kobe, Japan: Japan Welding Society.

15. Lord, M. 1999. Design and modeling of ultrahigh strength steel weld deposits. *Materials Science and Metallurgy*. University of Cambridge: Cambridge, U.K.

16. McRobie, D. E., and Knott, J. F. 1985. Effects of strain and strain aging on fracture toughness of C-Mn [steel] weld metal. *Materials Science and Technology* 1(5): 357–365.

17. Oldland, P. R., Ramsay, C. W., Matlock, D. K., and Olson, D. L. 1989. Significant features of high-strength steel weld metal microstructures. *Welding Journal* 68(4): 158-s to 168-s.

18. Svensson, L. E., and Gretoft, B. 1990. Microstructure and impact toughness of C-Mn steel weld metals. *Welding Journal* 69(12): 454-s to 461-s.

19. Taylor, D. S., and Evans, G. M. 1983. Development of MMA electrodes for offshore fabrication. *Met. Constr*. 15(8): 438–443.

20. Vassilaros, M. G., and Czyryca, E. J. 1992. The development of high-strength, cooling-rate insensitive ultralow-carbon steel weld metals. *Advances in Low-Carbon High-Strength Ferrous Alloys (LCFA-92)*. Jamshedpur; India: Trans Tech Publications Ltd.: Zurich, Switzerland.

21. Wang, W., and Liu, S. 2002. Alloying and microstructural management in developing SMAW electrodes for HSLA-100 steel. *Welding Journal* 81(7): 132-s to 145-s.

22. Farrar, R. A., and Harrison, P. L. 1987. Acicular ferrite in carbon-manganese weld metals: An overview. *J. Mater. Sci.* 22(11): 3812–3820.

23. Kang, B.Y., Kim, H. J., and Hwang, S. K. 2000. Effect of Mn and Ni on the variation of the microstructure and mechanical properties of low-carbon weld metals. *ISIJ International* (Japan) 40(12): 1237–1245.

24. Fairchild, D. P., Macia, M. L., Bangaru, N. V., and Koo, J. Y. 2003. Girth welding development for X120 linepipe in ISOPE-2003. *Thirteenth (2003) International Offshore and Polar Engineering Conference*. Honolulu, Hawaii. Cupertino, Calif.: International Society of Offshore and Polar Engineers.

25. Lord, M., and Jennings, G. 1999. Effect of interpass temperature on properties of high-

strength weld metals. *Svetsaren* (Sweden) 54(1-2): 53–58.

26. Bhadeshia, H. K. D. H. 1999. Neural networks in material science. *ISIJ International* (Japan) 39(10): 966–979.

27. Mackay, D. J. C. 1992. *Neural Computation*. p. 415.

28. Mackay, D. J. C. 1992. *Neural Computation*. p. 448.

29. Murugananth, M. 2002. Design of welding alloys creep and toughness. University of Cambridge: England.

30. Murugananth, M., Bhadeshia, H. K. D. H., Keehan, E., Andrén, H. O., and Karlsson, L. 2001. Strong and tough ferritic steel welds. *6th Int. Seminar Numerical Analysis of Weldability*. Schloss Seggau, Austria Institute of Materials, Minerals and Mining.

31. Keehan, E., Andrén, H. O., Karlsson, L., and Svensson, L.-E. 2006. New developments with C-Mn-Ni high-strength steel weld metals, Part B — Mechanical Properties. To be published in the *Welding Journal*.

32. SSAB, *WeldCalc.* 1998–99: Oxelösund, Sweden.

33. Keehan, E., Karlsson, L., and Andrén, H.-O. 2006. Influence of C, Mn, and Ni on strong steel weld metals: Part 1, Effect of nickel content. *Science and Technology of Welding and Joining* 11: 1–8.

34. Keehan, E., Karlsson, L., Andrén, H.-O., and Bhadeshia, H. K. D. H. 2006. Influence of C, Mn and Ni on strong steel weld metals: Part 2, Impact toughness gain from manganese reductions. *Science and Technology of Welding and Joining* 11: p. 9–18.

35. Keehan, E., Karlsson, L., Andrén, H.-O., and Bhadeshia, H. K. D. H. 2006. Influence of C, Mn and Ni on strong steel weld metals: Part 3, Increased strength from carbon additions. *Science and Technology of Welding and Joining* 11: p. 18–24.

36. Bhadeshia, H. K. D. H., Keehan, E., Karlsson, L., and Andren, H. O. 2006. Coalesced bainite. Accepted for publication in *Transactions of the Indian Institute of Metals*.

37. Padmanabhan, R., and Wood, W. E. 1984. *Materials Science and Engineering* 66: p. 1.

38. Chang, L. C., and Bhadeshia, H. K. D. H. 1996. Microstructure of lower bainite formed at large undercoolings below bainite start temperature. *Materials Science and Technology* 12(3): 233–236.

39. Keehan, E. 2004. Effect of microstructure on mechanical properties of high-strength steel weld metals. *Experimental Physics*. Chalmers University of Technology, Gothenburg, Sweden.

40. Sundman, B., Jansson, B., and Andersson, J.-O. 1985. *The* Thermo-Calc *Databank System*. Calphad 9(2): 153–190.

41. Honeycombe, R. W. K., and Bhadeshia, H. K. D. H. 1995. *Steel Microstructure and Properties*. 2 ed: Edward Arnold, London. p. 133.

42. Honeycombe, R. W. K., and Bhadeshia, H. K. D. H. 1995. *Steel Microstructure and Properties*. 2 ed: Edward Arnold, London. p. 103.

43. Takahashi, M., and Bhadeshia, H. K. D. H. 1990. A model for the transition from upper to lower bainite. *Materials Science and Technology* 6: 592–603.

44. Zhang, Z., and Farrar, R. A. 1997. Influence of Mn and Ni on the microstructure and toughness of C-Mn-Ni weld metals. *Welding Journal* 76(5): 183-s to 196-s.